scientific reports

Check for updates

OPEN

Preclinical models of melanoma leptomeningeal disease to assess intrathecal checkpoint blockade

Renato A. Guerrieri[1,2,9], Grant M. Fischer[1,2,3,9], Jacob R. Cortez[4], Barbara G. Knighton[1,2], Debora A. Ledesma[1], Courtney W. Hudgens[1], Yimmy F. Delcid[1,2], Qianghua Hu[1,2], Christian Y. B. Onana[1,2], Fernando C. L. Carapeto[1], Michael T. Tezlaff[1,5,6], Jason T. Huse[1,5], Patrick Hwu[2,7], Elizabeth M. Burton[8], Isabella C. Glitza Oliva[2,10], Michael A. Davies[1,2,8,10] & Sherise D. Ferguson[4,10]✉

Leptomeningeal disease (LMD) is a subtype of central nervous system metastatic disease that is associated with poor patient outcomes and limited treatment options. There is an unmet need to develop preclinical models of LMD to expedite and improve the development of new therapeutics. Here, we describe the development of multiple orthotopic immunocompetent murine models of melanoma LMD, including their use to assess the efficacy of systemic and/or intrathecal immunotherapy. LMD was established by direct intrathecal injection of murine cell lines (B16-F10, BP, D4M, D4M-UV2, MC38-gp100, RMS, YUMM3.1, and YUMMER1.7) into the cisterna magna of C57BL/6 mice. Tumor take rate, distribution, histology, peri-procedural mortality, and animal survival were assessed for each cell line. Intrathecal and systemic treatment with anti-PD1 were tested for safety, efficacy, and immune infiltration for LMD. Cisternal injection of murine melanoma cell lines successfully established LMD with low peri-procedural mortality, high tumor take rate, and varied survival duration across the panel of cell lines. Decreasing the total number of cells injected and increasing the volume of suspension of the injected cells increased the rate of distal spinal cord deposits, reflecting the common clinical distribution of LMD. Intrathecal administration of anti-PD1 in non-tumor bearing mice caused no morbidity or toxicity. Concurrent intrathecal and systemic anti-PD1 immunotherapy increased the survival of mice with murine melanoma LMD. We have established and characterized several immunocompetent murine models of LMD to facilitate the development and testing of new, more effective immunotherapy strategies for melanoma patients with LMD.

Keywords Leptomeningeal disease, Melanoma, Intrathecal, anti-PD1, Immunotherapy

Abbreviations

LMD	Leptomeningeal disease
CSF	Cerebrospinal fluid
CNS	Central nervous system
ICI	Immune checkpoint inhibitor
IT	Intrathecal
IL-2	Interleukin-2
ICP	Intracranial pressure
IV	Intravenous
IP	Intraperitoneal

[1]Department of Translational Molecular Pathology, The University of Texas MD Anderson Cancer Center, Houston, TX, USA. [2]Department of Melanoma Medical Oncology, The University of Texas MD Anderson Cancer Center, Houston, TX, USA. [3]Department of Pathology, Brigham and Women's Hospital, Boston, MA, USA. [4]Department of Neurosurgery, The University of Texas MD Anderson Cancer Center, Houston, TX, USA. [5]Department of Pathology and Laboratory Medicine, The University of Texas MD Anderson Cancer Center, Houston, TX, USA. [6]Department of Pathology, University of California San Francisco, San Francisco, CA, USA. [7]Department of Cutaneous Oncology, Moffitt Cancer Center, Tampa, FL, USA. [8]Department of Genomic Medicine, The University of Texas MD Anderson Cancer Center, Houston, TX, USA. [9]Renato A. Guerrieri and Grant M. Fischer contributed equally as first authors. [10]Isabella C. Glitza Oliva, Michael A. Davies and Sherise D. Ferguson contributed equally as senior authors. ✉email: SDFerguson@mdanderson.org

H&E	Hematoxylin and eosin
IHC	Immunohistochemistry
BLI	Bioluminescence imaging

Leptomeningeal disease (LMD) is a devastating complication of advanced cancer in which tumor cells disseminate to the cerebrospinal fluid (CSF) and/or leptomeninges. The spread of cancer cells into the CSF can lead to dissemination throughout the entire central nervous system (CNS) and may result in a variety of neurologic symptoms that can dramatically impact patient quality of life. The incidence of LMD is rising which is likely due to longer survival of cancer patients and improved imaging techniques have enhanced the ability to detect this increased incidence[1] Metastatic melanoma has a particularly high propensity for leptomeningeal dissemination where 5–7% of all metastatic melanoma patients are diagnosed with LMD[2–5]. Importantly, LMD portends a very poor prognosis. Our retrospective study of 178 melanoma patients diagnosed with LMD patients reported a median overall survival of only 3.5 months from diagnosis[6]. Further, our recent analysis of 791 metastatic melanoma patients diagnosed with CNS metastases showed that the presence of LMD is one of the most significant prognostic factors in the current era of immunotherapy.

Recent clinical trials with immune checkpoint inhibitors (ICIs) in patients with parenchymal brain metastases have demonstrated intracranial efficacy and overall survival benefit[7–9]. These studies support the inclusion of patients with CNS metastasis in prospective clinical trials with ICIs. However, melanoma patients with LMD have continued to be excluded from these and virtually all other clinical trials. Thus, there is a critical need to develop new clinical trials specifically for patients with LMD. Our group previously reported prolonged survival (> 5 years) in approximately 15% of melanoma LMD patients treated at our institution with intrathecal (IT) interleukin-2 (IL-2) immunotherapy[10]. However, IT IL-2 had 100% incidence of severe toxicities, requiring patients to be hospitalized for ~ 4 weeks to manage symptoms caused by increased intracranial pressure (ICP) caused by this therapy. Building upon this experience, and the general advancement of immunotherapy for this disease, recently we reported the initial results of a first-in-human phase I/Ib clinical trial designed to evaluate the safety and preliminary efficacy of concurrent IT and intravenous (IV) nivolumab in melanoma patients with melanoma LMD. The results from the dose escalation portion of the study demonstrated that IT + IV nivolumab was safe and established a recommended phase II dose of 50 mg IT nivolumab[11]. Despite the fact that ~ 90% of the patients had previously progressed on IV immune checkpoint inhibitor (ICI) immunotherapy, several patients achieved radiographic responses and symptomatic benefit, and the median OS to date is a promising 7.5 months[12]. Combined with the excellent safety profile of IT + IV nivolumab, these initial results indicate that IT ICI immunotherapy may be a promising therapeutic strategy for patients with melanoma LMD. However, there is a need to build upon these initial results to identify strategies with even greater efficacy- which will be facilitated by improving our understanding of the predictors and mechanisms of resistance to this approach through the use of preclinical models.

Despite the importance of preclinical models in advancing our understanding of LMD and guiding the development of new therapeutic strategies, several challenges exist in their establishment and utilization. One significant challenge is the limited availability of human specimens for the development of patient-derived xenograft (PDX) models. Obtaining suitable patient-derived samples, particularly from the CSF or leptomeningeal metastatic lesions, can be logistically difficult. Moreover, the successful engraftment and propagation of human tumor cells in immunodeficient mouse hosts require careful optimization and may not fully recapitulate the complex interactions between tumor cells and the host immune system seen in clinical LMD. Furthermore, the time and resources required to establish and characterize preclinical models, including murine models, can be substantial, limiting the scalability and accessibility of these approaches for widespread use in research and drug development. As such, we set out to overcome the challenges associated with establishing murine models by defining the cell preparation and injection conditions for this approach to modeling LMD.

Developing effective strategies for LMD will be facilitated and accelerated by the establishment and characterization of additional clinically relevant preclinical models. Previous approaches for the study of LMD have included direct orthotopic implantation of tumor cell lines into the cisterna magna, orthotopic patient-derived xenografts, and iterative in vivo selection to generate LMD-tropic cell lines[13–16]. To date, preclinical models have not been employed for the study of immune therapies. The availability of such models will allow for testing of new IT immunotherapy regimens to help select and prioritize strategies for clinical development. Further, such models will provide opportunities for research that are not feasible in patients to study the pathogenesis of LMD and mechanisms of resistance to different therapeutic approaches. To address this gap, we have developed and optimized several immunocompetent orthotopic murine models of melanoma LMD. We have also used these models to evaluate the feasibility and safety of ICI therapy, including a preliminary assessment of the therapeutic efficacy of this approach in these models. Our results establish new resources to support LMD research and to accelerate the development of new immunotherapy approaches for this disease.

Materials and methods

Animals

The Institutional Animal Care and Use Committee of The University of Texas MD Anderson Cancer Center approved all procedures and experiments involving animals. The study is reported in accordance with ARRIVE guidelines (https://arriveguidelines.org). All methods were carried out in accordance with relevant guidelines and regulations. All animal experiments were performed using C57BL/6J mice (8–10 weeks old; Jackson) at the MD Anderson South Campus Animal Vivarium.

Cell lines

Luciferase-tagged B16-F10 (generously provided by Dr. Willem Overwijk), BP (generously provided by Dr. Weiyi Peng), D4M and D4M-UV2 (generously provided by Dr. David Fisher), and RMS (generously provided by Dr. Neta Erez) murine melanoma cell lines and luciferase-tagged MC38-gp100 murine colorectal carcinoma cell line (generously provided by Dr. Weiyi Peng) were grown in DMEM media supplemented with glutamine and 10% heat-inactivated fetal bovine serum (FBS) (Corning). Luciferase-tagged YUMMER1.7 and YUMM 3.1 murine melanoma cell lines (generously provided by Dr. Marcus Bosenberg) were grown in DMEM/F12 (50:50) media supplemented with 1% non-essential amino acids and 10% heat-inactivated FBS (Corning). All cell lines were grown at 37 °C under 5% CO_2. All cell lines were confirmed negative for mycoplasma prior to initiating experiments using the MycoAlert Mycoplasma Detection Kit (Lonza) according to the manufacturer's specifications.

Therapeutics

Isotype rat IgG2a anti-trinitrophenol control antibody (Company: BioXCell, Clone: 2A3, #BE0089) and anti-mouse PD1 antibody (Company: BioXCell, Clone: RMP1-14, #BE0146) were purchased to evaluate the safety and efficacy of IT and systemic anti-PD1 administration and the combination of systemic and IT anti-PD1. All therapeutic antibodies were diluted in PBS under sterile conditions.

Cisterna magna (intrathecal) injection technique for LMD modeling and treatment

The entire dorsal surface of the mouse head and neck was shaved with an electric razor. Mice were anesthetized with an intraperitoneal (IP) injection of ketamine/xylazine cocktail (80 mg/kg ketamine and 12 mg/kg xylazine). Percutaneous IT injection was performed with a 30-gauge Hamilton needle with precision to 0.1 µL. To perform the injection, mice were placed in the prone position with the neck flexed over a 15 mL conical centrifuge tube. The head was immobilized with the thumb and index finger. The space between the occiput and the C1 vertebrae was palpated, and the entry point was marked on the skin. The needle was inserted to a marked depth of 4 mm at a 45° angle[13]. The solution was dispensed slowly over 1 min into the cisterna magna, and the needle was then withdrawn. The mice were then resuscitated from anesthesia. In our initial LMD model, we injected 1.5×10^4 murine melanoma cells diluted in 10 µL HBSS. After optimization of our model, the IT injection conditions were modified to 2.0×10^3 cells diluted in 20 µL HBSS. For both cell suspension volumes, mice were monitored for any signs of discomfort or other adverse effects, including changes in behavior, posture, or mobility.

Safety evaluation of IT anti-PD1

In our initial IT treatment efficacy studies, we injected 13 µg anti-PD1 or isotype control diluted in 6.5 µL PBS into non-tumor-bearing mice. As previously described, antibody drug solution of 6.5 µL is consistent with physiologic IT dosing in mice[11]. We performed additional studies evaluating the safety of higher anti-PD1 doses (26–39 µg anti-PD1 in 6.5 µl PBS) compared with isotype control or PBS in non-tumor bearing mice. For all doses, mice were monitored for changes in body weight measurement as well as any signs of discomfort or other adverse effects, including changes in behavior, posture, or mobility. After completing these safety studies, the IT treatment conditions were modified to 39 µg anti-PD1 or isotype control in 6.5 µl PBS.

In vivo bioluminescence imaging (BLI)

At selected time points, D-luciferin sodium salt (BioVision #7902) was injected at 150 mg/kg into the peritoneum of each mouse. After 10 min, the animal was placed in an IVIS100 in vivo imager and scanned on default settings, with the exception that exposure time was automatically determined by the Living Image (v4.5.2) software. The bioluminescence image was overlaid onto a photographic image for anatomical location of the signal. Signal intensities were quantified using Living Image (v4.5.2) software. Regions of interest were automatically determined by the software. The minimum percentage of peak pixel intensity for inclusion was set to 20%. Values were normalized against a black surface in the image and a non-luminescent surface of an animal. Total flux values were exported into Microsoft Excel 2016 and Prism 8.0 (GraphPad) for downstream analysis.

Tissue analyses

Mice were euthanized via CO_2 inhalation and cervical dislocation. The brain and vertebral column were removed, fixed in 10% buffered formalin for 48 h, and transferred to 70% ethanol until processing. Brains were sectioned coronally at 2 mm increments when preparing tissue for processing. Spinal cords were dissected from the vertebral column and processed in their entirety. Brain regions and spinal cords were embedded in paraffin and sectioned at 5 µm and stained with hematoxylin and eosin (H&E) for histological observation. All immunohistochemistry (IHC) studies were performed on 5 µm sections.

For immune cell populations, slides were stained with antibodies targeting anti-mouse CD8 (Cell Signaling #98941; 1:400) using a modified version of the standard Leica Bond red "J" IHC protocols. The data were expressed as a density (total number of IHC-positive cells/mm^2 area).

Anti-mouse Melan-A/MART-1 antibody (Novus Biologicals #A19-P, 1:600) or anti-mouse gp100 antibody (Cell Signaling #38815, 1:1000) was used to confirm the presence of melanoma in leptomeningeal deposits in animal specimens. An Aperio ScanScope was used to take pictures, which were then processed with Aperio ImageScope (Leica Biosystems). All slides were reviewed by three pathologists, including: a neuropathologist (J.H.); a dermatopathologist who specializes in the assessment of inflammatory markers and responses (M.T.); and a veterinary pathologist (F.C.).

Cell enumeration by crystal violet staining

Eight cell lines (D4M, D4M-UV2, B16, MC38gp100, RMS, BP, YUMMER1.7, YUMM3.1) used for our LMD models were cultured in DMEM + 10% FBS + 1% Non-essential Amino Acids. In vitro cell growth patterns between them were compared with crystal violet (Sigma-Aldrich) staining every 24 h post cell inoculation in 24-well plates. The experimental protocol described previously.[17] The crystal violet absorbance at a wavelength of 590 nm representing relative viable cells was measured on a plate reader and the cell growth curves were plotted with the best-fit program of GraphPad Prism 10. To achieve the same baseline reading 24 h post cell inoculation, 1400 cells/well for D4M, D4M-UV2, B16, MC38gp100, RMS but 2000 cells/well for BP, YUMMER1.7, and 2500 cells/well for YUMM3.1 were inoculated. Each cell line had 4 replications or wells.

Efficacy experiments

For our initial efficacy experiments, 1.5×10^4 luciferase-tagged B16-F10 cells suspended in 10 µl HBSS were directly injected into the cisterna magna of C57BL/6 mice. After 3 days, mice underwent BLI to confirm tumor uptake and were then randomized to receive: (1) IT isotype control antibody + systemic isotype control antibody; (2) IT isotype control antibody + systemic anti-PD1 antibody; (3) IT anti-PD1 antibody + systemic isotype control antibody; (4) IT anti-PD1 antibody and systemic anti-PD1 antibody. Initially IT treatments were given as a single 13 µg injection (prepared in 6.5 µl of PBS) into the cisterna magna, and systemic treatments were given intraperitoneally three times per week at a flat dose of 200 µg/mouse for up to 4 weeks. Mice were weighed every two days. Mice were euthanized if they had ≥ 20% weight loss, displayed neurological symptoms (ataxia, seizures, or paralysis), or were moribund. Mice underwent weekly BLI and were tracked for a total of up to 180 days from treatment initiation.

Efficacy experiments were repeated using our diluted model conditions, in which 2.0×10^3 cells suspended in 20 µL HBSS were injected into the cisterna magna of C57BL/6 mice. Due to limited bioluminescence signal three days post-implantation in the optimized diluted model, mice with positive signal were randomized into treatment groups; mice with negative signal were evenly distributed among treatment groups. Intrathecal treatments were given as a single 39 µg injection (anti-PD1 or isotype control); systemic treatments were given as intraperitoneal injections of 200 µg (anti-PD1 or isotype control) three times per week for up to four weeks. Mice were monitored and euthanized as described above.

Statistical analysis

Overall survival was defined as the interval from date of treatment initiation to date of death. Survival duration was analyzed by Kaplan-Meier method. Survival curves were drawn in Prism 8.0 (GraphPad). Hazard ratios and significance were calculated via the Mantel-Haenszel test and log-rank test, respectively, in Prism 8.0 (GraphPad). Data analyses and representations were performed via Prism 8.0 (GraphPad). Comparison of continuous variables between two groups was performed by unpaired Student's *t*-tests. Evaluation of associations between categorical variables was evaluated by Fisher's exact test. All statistical significance testing was two-sided at Type-I error rate of 0.05.

Results

Establishing a model of B16-F10 murine melanoma LMD via percutaneous IT injection in immunocompetent mice

To establish a model of melanoma LMD in immunocompetent mice, we performed a percutaneous IT injection to access the cisterna magna (Figure S1). This route was chosen because it allows direct access to the CSF compartment for the delivery of melanoma cells. We previously described the viability of this technique by confirming the distribution of injected material to the subarachnoid space/leptomeninges using IT injection of Evans (methylene) blue dye into C57BL/6 mice[11].

In initial experiments we injected 1.5×10^4 luciferase-tagged B16-F10 cells (diluted in 10 µL HBSS) into the cisterna magna of C57BL/6 mice. No symptoms of pain or discomfort were observed in mice before, during, or after injection of cell suspension for all experiments. Three days post-injection, mice were injected with luciferin and imaged twice per week in order to detect in vivo bioluminescence imaging (BLI) and confirm tumor presence and growth (Fig. 1A-B). At the time of animal deaths, brain and spinal cord tissues were collected. Gross inspection demonstrated the presence of leptomeningeal B16-F10 deposits to the spinal cord and subarachnoid space, including the lateral ventricles and base of the pial surface of the brain stem (Fig. 1C). B16-F10 tumor deposits were confirmed histologically by H&E staining and by IHC for the melanoma marker MART1 (Fig. 1D-E).

Characterization of additional cell line models of LMD

We then tested additional murine melanoma cell lines, including BP, D4M, D4M-UV2, RMS, YUMMER1.7, and YUMM3.1, for the ability to establish LMD and mouse survival (Table S1). In addition, we evaluated the colon adenocarcinoma cell line MC38-gp100 given its frequent use as a model in preclinical immunotherapy studies[18]. Consistent with our B16-F10 experiments, we administered cisternal injections of 1.5×10^4 cells for each cell line.

We recorded peri-procedural mortality, post-implantation in vivo BLI signal at three days post-injection, overall survival, and rate of formation of distal spinal cord deposits at time of death for each LMD model (Table S2). Peri-procedural mortality associated with cisternal injection for all cell lines ranged from 10% − 28.6% (Fig. 2A). In vivo BLI signal three days post-injection was 100% for mice injected with B16-F10, RMS, and YUMM3.1; injection of all other cell lines resulted in BLI positive tumor signal in 75–80% mice at this timepoint (Fig. 2B). All mice were positive for BLI signal at seven days post-injection for all cell lines. We observed complete tumor regression (BLI signal disappearance) of YUMMER1.7 tumors in 40% of mice (Figure S2). Immune-

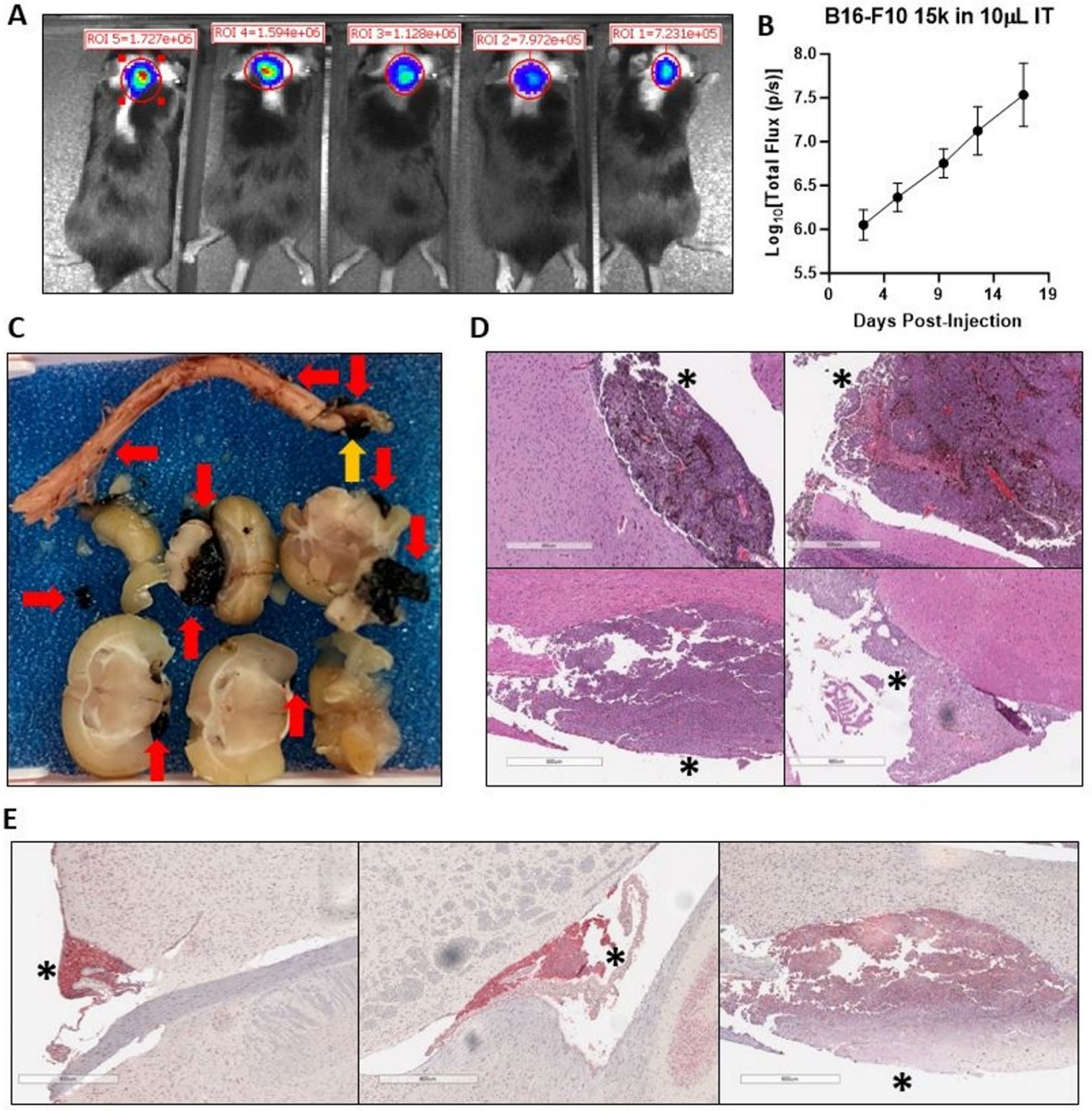

Fig. 1. IT injection of B16-F10 melanoma (1.5 × 10^4 in 10 µL suspension) produces LMD in C57BL/6 mice. (**A**) Bioluminescence imaging (BLI) of C57BL/6 mice injected with 1.5 × 10^4 (15 K) luciferase-tagged B16-F10. All mice had positive signal at day 3 post-IT injection. (**B**) Line graph showing BLI flux signal post-injection of 15 K luciferase-tagged B16-F10. (**C**) Gross photographs of C57BL/6 mice after IT injection of 15 K B16-F10 in 10 µL suspension. Red arrows indicate spinal cord (top) and cranial melanoma deposits; yellow arrow indicates tumor deposit at site of IT injection. (**D**) Representative H&E slides at 4X magnification from C57BL/6 mice after IT injection of 15 K B16-F10 in 10 µL suspension. Asterisks (*) denote LMD deposits in the spinal cord (lower left) and brain cortex (all others). (**E**) Representative slides with IHC stain for melanoma marker MART1 at 4X magnification from C57BL/6 mice after IT injection of 15 K B16-F10 in 10 µL suspension. Asterisks (*) denote MART1 positive LMD deposits. Far left: cranial cortex; center: intraventricular; far right: spinal cord.

mediated spontaneous regression of YUMMER1.7 tumors in immunocompetent mice has been reported elsewhere, therefore we did not pursue further LMD modeling with YUMMER1.7. All mice were maintained until > 20% weight loss or neurologic symptoms were observed. At the time of animal death, we collected brain and spinal cord tissues for H&E staining (Figure S3) and IHC for MART1 (Figure S4). Survival varied across the different LMD models, with median overall survival ranging from 13 to 48 days (Fig. 2C). In addition to

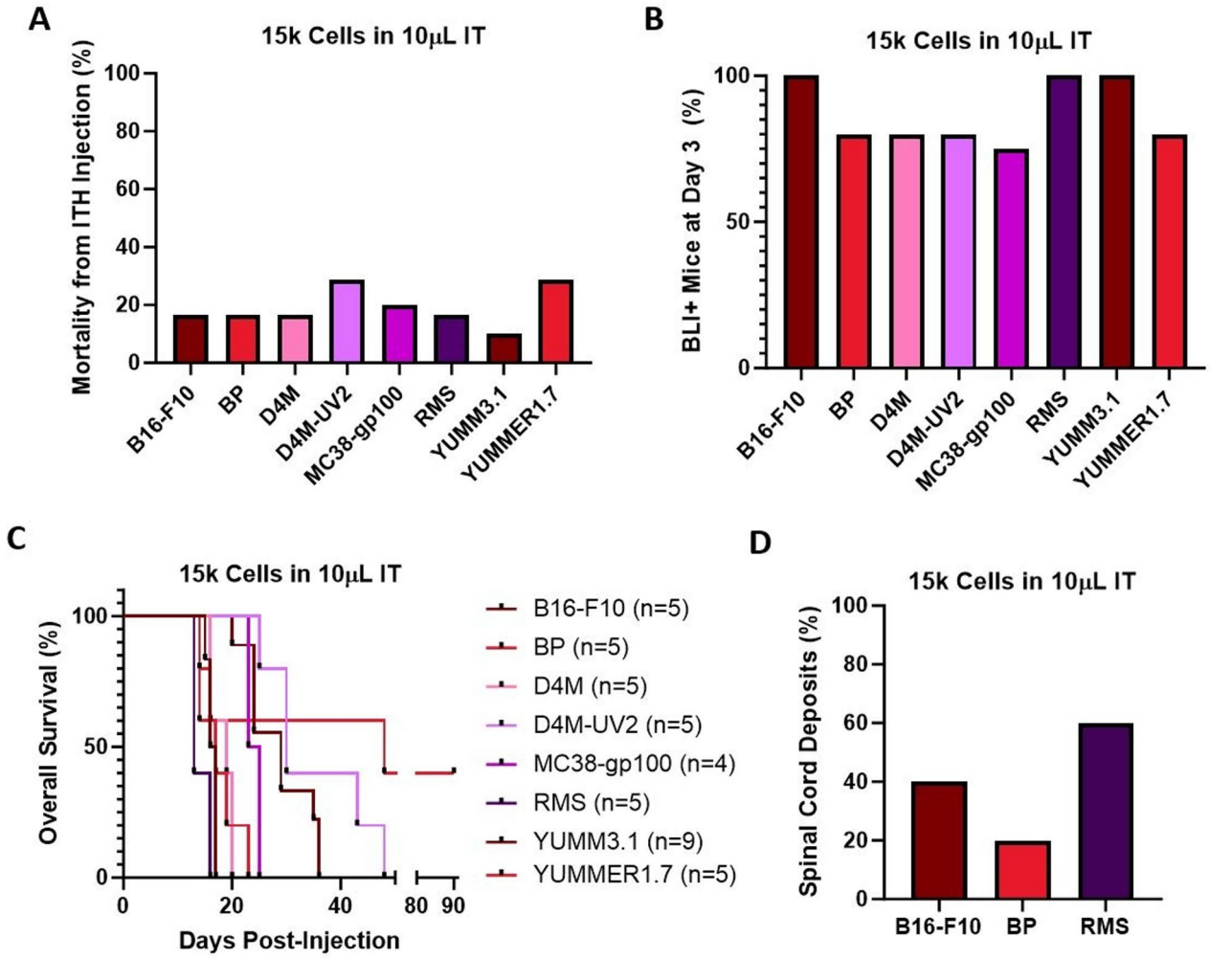

Fig. 2. IT injection (15 K in 10 μL suspension) of syngeneic melanoma cell lines produce LMD in C57BL/6 mice. (**A**) Bar chart showing peri-procedural mortality following IT injection of 15 K in 10 μL suspension of melanoma cell lines and MC-38 (colon cancer cell line). $N = 5$ for B16-F10, BP, D4M, D4M-UV2, RMS, YUMMER1.7; $N = 9$ for YUMM3.1; $N = 4$ for MC38-gp100. X-axis indicates cell line. Y-axis indicates percentage of mice dying following IT injection of 15 K cells in 10 μL suspension. (**B**) Bar chart showing BLI positivity following IT injection of 15 K melanoma cell lines in C57BL/6 mice. X-axis indicates cell line. Y-axis indicates percentage of mice with BLI positive signal at day 3 post IT injection. (**C**) Survival curves following IT injection of 15 K in 10 μL suspension of melanoma cell lines. (**D**) Bar chart showing the percentage of spinal cord deposits in post-mortem C57BL/6 mice following IT injection of 15 K in 10 μL suspension of pigmented cell lines, B16-F10, BP and RMS.

tumor deposits in the cranial compartment, 20–60% of mice developed tumor deposits along the spinal cord that were distal to the injection site following injection with B16-F10, BP, or RMS cells consistent with diffuse leptomeningeal spread (Fig. 2D). To determine whether the in vivo growth rate of the evaluated melanoma cell lines corresponded to the proliferation rate of these same cell lines in vitro we performed a proliferation assay with crystal violet staining (Figure S5). Similar to the in vivo data, RMS remained the most aggressive cell line with the shortest doubling time. YUMMER1.7 remained the among the less aggressive cell lines overall. Notably D4M-UV2 had one of the higher proliferation rates in vitro but was one of the less aggressive LMD models. Similarly, B16 was one of the most aggressive LMD models but had a moderate proliferation rate in vitro. This may indicate that some lines have a higher propensity of growth in the intrathecal space that is beyond just the cell proliferation rate.

Diluted cell suspension IT injection facilitates distribution of cranial and spinal cord LMD deposits.

In our initial model we observed a predominance of bulky tumor deposits in the cranial compartment after IT injection of 1.5×10^4 cells. While this can be observed in some patients with LMD, smaller more widely distributed tumor deposits throughout the CNS are more common. As such, we initiated experiments to improve the spinal cord and cranial distribution of tumor deposits from IT injection to better represent the clinical disease. We

attempted to optimize our models by altering the cell concentration at injection to reduce cell clumping in the cisterna magna from IT injection and facilitate enhanced distribution of tumor cells through the CNS. As bulky disease may result in increased acute symptomatology necessitating euthanasia, our secondary objective was to develop preclinical LMD models with lengthened overall survival in order to extend the therapeutic window for treatment experiments.

We evaluated tumor distribution and overall survival in B16-F10, BP, and RMS after IT injection of 1×10^3, 2×10^3, 5×10^3, and 1.5×10^4 cells in both 10 µL and 20 µL suspensions (Figure S6). Overall, we found that injection of 2×10^3 murine melanoma cells in a 20 µL HBSS resulted in consistent formation of both cranial and spinal cord deposits, and hereby refer to this technique as our diluted LMD model. Three days after injection of B16-F10 cells, mice were evaluated to detect in vivo BLI and confirm tumor presence (Fig. 3A-B). Upon harvest, gross inspection demonstrated the presence of B16-F10 tumor deposits in the cranial compartment and spinal cord, including in areas distal to the IT injection site (Fig. 3C). B16-F10 tumor deposits were confirmed histologically by H&E staining and IHC for MART1 (Fig. 3D-E).

We then characterized each cell line for peri-procedural mortality, in vivo BLI signal at three days post-injection, overall survival, and rate of distal spinal cord deposits at time of death using the diluted LMD model conditions. We observed no peri-procedural mortality for mice injected with BP, MC38-gp100, RMS, and YUMM3.1; peri-procedural mortality associated with IT injection of B16-F10 and D4M was 10% for each, and 20% for D4M-UV2 (Fig. 4A). In vivo BLI signal three days post-injection was 100% for mice injected with B16-F10 and RMS, and 50–80% for the other cell lines (Fig. 4B). BLI signal was 100% in all LMD models at day seven post IT injection. At the time of animal death, we collected brain and spinal cord tissues for H&E staining (Figure S7) and IHC for MART1 (Figure S8) for each LMD model. Survival across LMD models varied, with median overall survival ranging from 21 to 76 days (Fig. 4C), which was increased compared to our initial LMD model conditions. B16-F10 and RMS had the shortest median overall survival (range 21–22 days); BP, D4M, and YUMM3.1 had intermediate survival (median range 38.5–43 days); D4M-UV2 and MC38-gp100 had the longest survival (median range 72.5–76 days). All mice injected with B16-F10, BP, or RMS developed tumor deposits along the spinal cord distal to the injection site in addition to tumor deposits at the injection site and throughout the brain (Fig. 4D). When comparing the diluted LMD model with our initial model, the diluted model significantly improved the rate of distal spinal cord deposits in the B16-F10 ($p=0.011$) and BP ($p<0.001$) models and trended towards improvement for RMS ($p=0.087$). Thus, cisternal injection of 2×10^3 cells in a 20 µL cell suspension had low peri-procedural mortality, varied overall survival between models (with longer survival than initial model), and increased CNS distribution of tumor deposits demonstrated by increased spinal cord deposits post IT injection (Table S3).

Intrathecal anti-PD1 to treat melanoma LMD in initial preclinical model

We then used our murine LMD models to evaluate the efficacy of systemic intraperitoneal (IP) and IT anti-mouse PD1. For our pilot evaluation, we assessed the effects of IT anti-PD1 treatment in mice with B16-F10 LMD. Notably, we previously evaluated an IT dose of 13 µg anti-PD1 in 6.5 µL PBS, which is equivalent to a dose of 50 mg in patients based on differences in CSF volumes in mice versus humans, and which we established as the recommended IT dose of nivolumab in our phase I trial[11]. We demonstrated that 13 µg anti-PD1 in 6.5 µL could safely be administered via IT injection in non-tumor-bearing C57BL/6 mice, consistent with our previous report[11]. Here, C57BL/6 mice were injected IT with 1.5×10^4 B16-F10 cells to establish LMD. Three days post B16-F10 IT injection, mice were evaluated for tumor BLI signal. Animals with confirmed tumor were randomized into four treatment groups that were equivalent in mean total flux: Group 1 was treated with one-time IT isotype control antibody + IP isotype control antibody; Group 2 was treated with one-time IT isotype control antibody + IP anti-PD1 antibody; Group 3 was treated with one-time IT anti-PD1 antibody + IP isotype control antibody; Group 4 was treated with one-time IT anti-PD1 antibody and IP anti-PD1 antibody. IT treatments were given at a dose of 13 µg once on day 0 (day of randomization); IP treatments were given at a dose of 200 µg/mouse (IP) on days, 0, 2, and 5 (Figure S9).

Mice treated with IT and IP isotype control had a median overall survival of 9 days from the start of treatment; all mice in this group were euthanized by day 14 due to significant morbidity (Fig. 5A). Treatment with IT anti-PD1 alone demonstrated a trend for improved overall survival versus the control treatment (HR 0.392, $p=0.097$), with 22.2% mice surviving more than 28 days. IP anti-PD1 alone also showed a trend for improved overall survival (HR = 0.346, $p=0.072$), with 33.3% of mice surviving more than 28 days, and 10.0% of mice surviving > 6 months. Combined treatment with IT anti-PD1 and IP anti-PD1 was the only treatment that significantly improved survival versus controls (HR = 0.269, $p=0.023$), with 40.0% mice surviving more than 28 days, and 20.0% mice alive > 6 months. The experiment was repeated, and again combination treatment with IT anti-PD1 and IP anti-PD1 achieved the best outcomes and was the only treatment to significantly improve survival (Figure S10).

At the endpoint, brain and spinal cord tissues were processed for translational studies from each treatment group. IHC demonstrated that each treatment significantly increased the $CD8^+$ T-cell infiltrate in LMD deposits compared with the isotype control-only arm (Fig. 5B**).** There were no significant differences observed between the anti-PD1-containing treatment groups.

Intrathecal anti-PD1: results in diluted LMD model

Next, we evaluated anti-PD1 efficacy using the diluted LMD model conditions. C57BL/6 mice were injected IT with 2.0×10^3 B16-F10 cells (in 20 µL HBSS) to establish LMD. In these experiments we used an escalated one-time dose of IT anti-PD1 (39 µg), as pilot experiments in non-tumor bearing mice showed no additional weight loss or toxicity compared to 13 µg (Figure S11), similar to the lack of toxicity we observed with increasing IT nivolumab doses in our recent clinical trial[11]. We also administered IP anti-PD1 treatments three times per week

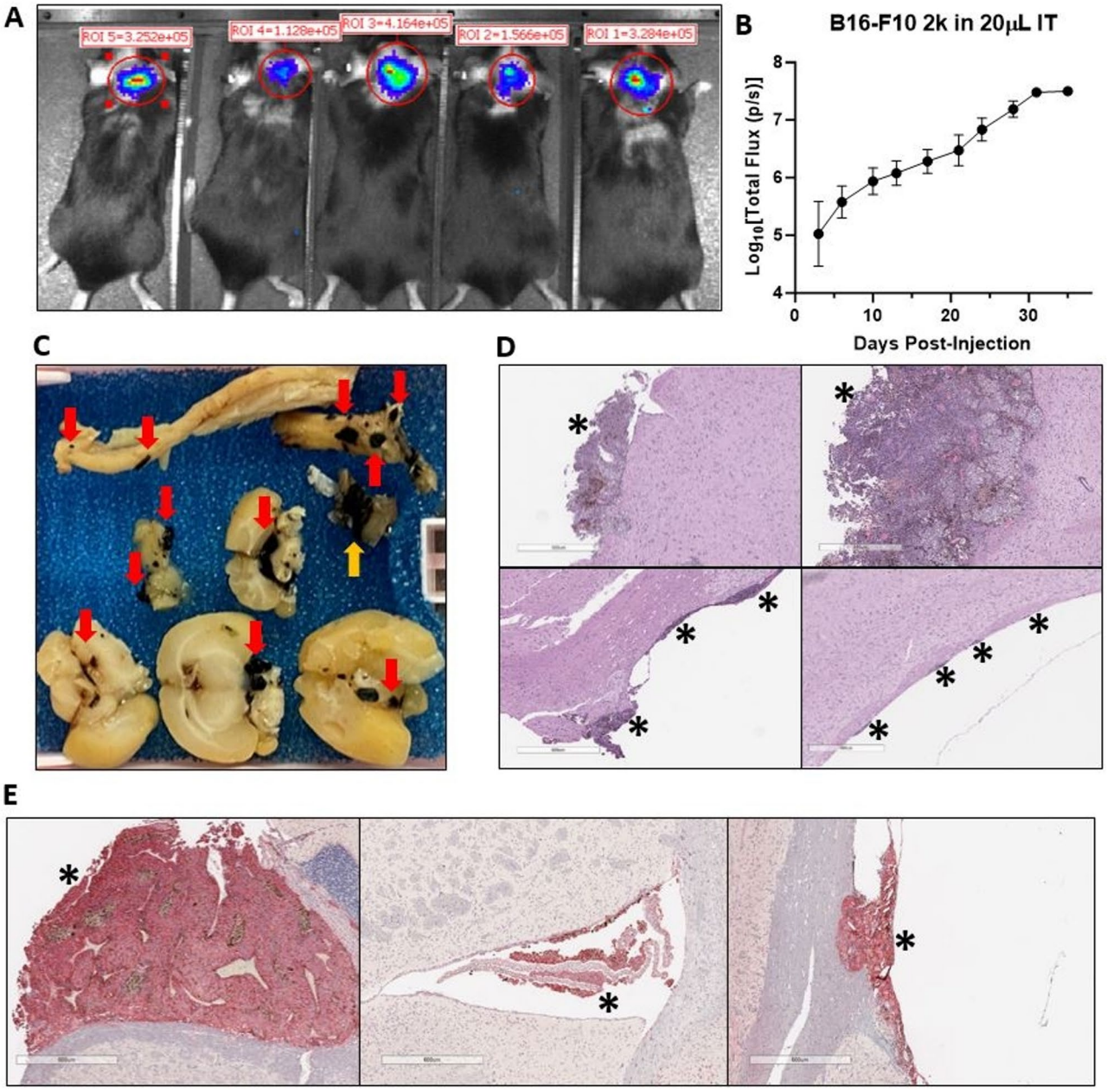

Fig. 3. Development of optimized LMD model with IT injection (2 K in 20 µL suspension) of B16-F10 melanoma. (**A**) BLI of C57BL/6 mice injected with 2.0 × 10^3 (2 K) luciferase-tagged B16-F10 in 20 µL suspension. All mice had positive signal at day 3 post-IT injection. (**B**) Graph showing BLI flux signal per day post injection of 2 K luciferase-tagged B16-F10. (**C**) Gross photographs of C57BL/6 mice after IT injection of 2k B16-F10 in 20 µL suspension. Arrows show black spinal (top) and cranial melanoma deposits. (**D**) Representative H&E slides at 4X magnification from C57BL/6 mice after IT injection of 2k B16-F10 in 20 µL suspension. Asterisks (*) denote LMD deposits. Upper panels cranial cortex deposits; lower panels spinal cord. (**E**) Representative slides with IHC stain for melanoma marker MART1 at 4X magnification from C57BL/6 mice after IT injection of 2k B16-F10 in 20 µL suspension. Asterisks (*) denote MART1 positive LMD deposits. Far left: cranial cortex; center: intraventricular; far right: spinal cord.

for up to four weeks (Figure S12). Three days after B16-F10 IT injection, mice were randomized into the four treatment groups as used above. Mice with no BLI signal by day 3 were evenly distributed between treatment groups (all mice eventually formed tumors positive for BLI signal).

Animals treated with IT and IP isotype control had a median overall survival of 21 days from the start of treatment; all mice in this group were euthanized by day 28 due to significant morbidity (Fig. 6A). IP anti-PD1 alone did not improve overall survival (HR = 0.841, $p = 0.681$), although 13.3% mice were alive at 28 days and 6.7% survived > 6 months. IT anti-PD1 alone improved survival versus controls (HR = 0.265, $p = 0.005$), with

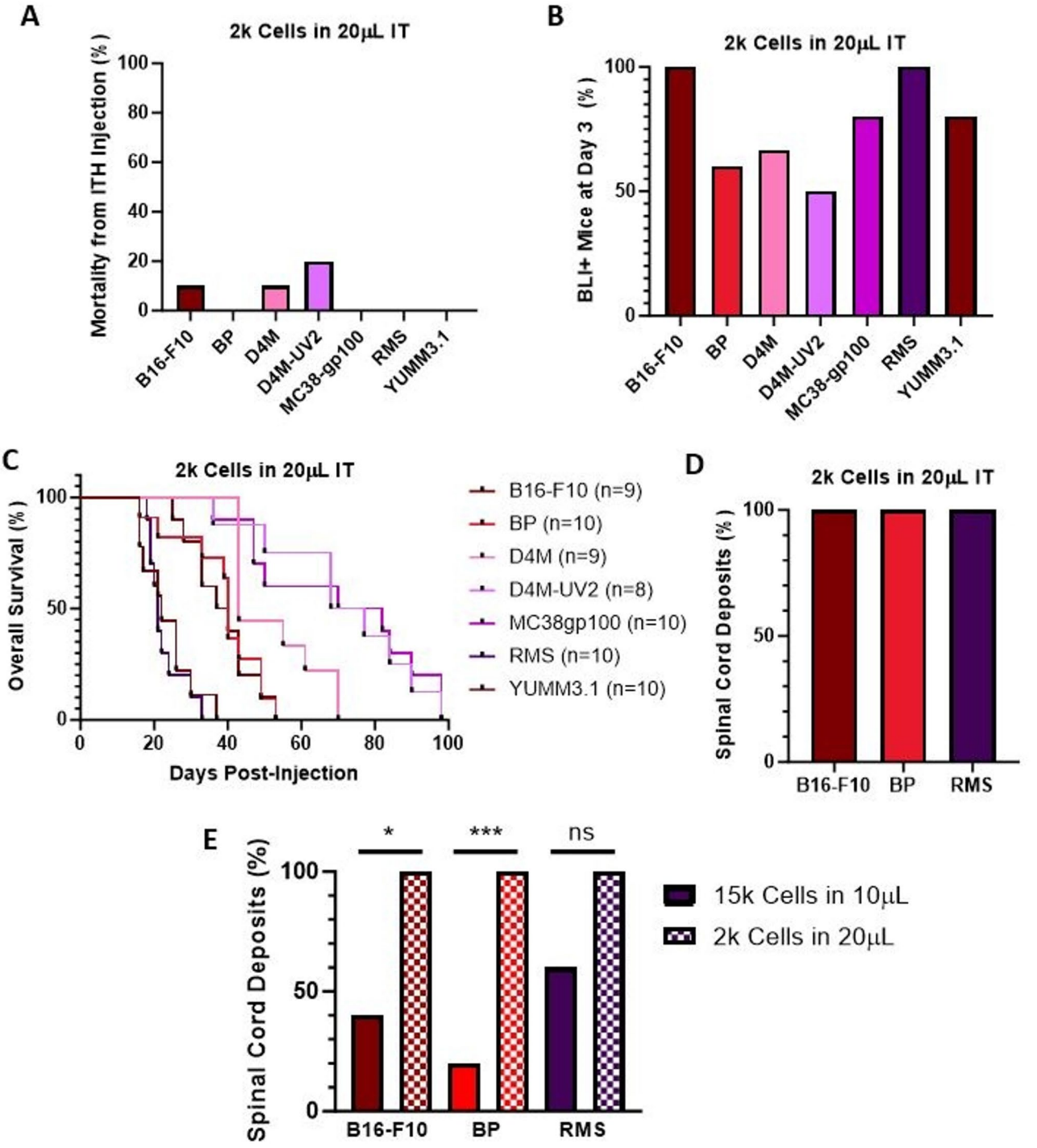

Fig. 4. Optimized LMD model with IT injection (2 K in 20 µL suspension) of syngeneic melanoma cell lines. (**A**) Bar chart showing peri-procedural mortality following IT injection of 2k in 20 µL suspension of melanoma cell lines and colon cancer line MC-38. $N = 9$ for B16-F10, D4M; $N = 10$ for BP, MC38-gp100, RMS, YUMM3.1; $N = 8$ for D4M-UV2. X-axis indicates cell line. Y-axis indicates percentage of mice dying following IT injection. (**B**) Bar chart showing BLI positivity following IT injection of 2 K melanoma cell lines in of C57BL/6 mice. (**C**) Survival curve for following IT injection of 2 K in 20 µL suspension of melanoma cell lines and MC-38. (**D**) Bar chart showing the percentage of spinal cord deposits in post-mortem C57BL/6 mice following IT injection of 2 K in 20 µL suspension of B16-F10, BP and RMS cell lines. (**E**) Bar graph comparing spinal cord distribution in the 15 K in 10 µL suspension versus 2 K in 20 µL suspension. Significantly higher spinal cord distribution was observed in the optimized diluted model in the B16-F10 and BP models. $^{***}p < 0.001$, $^{*}p < 0.05$ by two-sided Student's *t*-test.

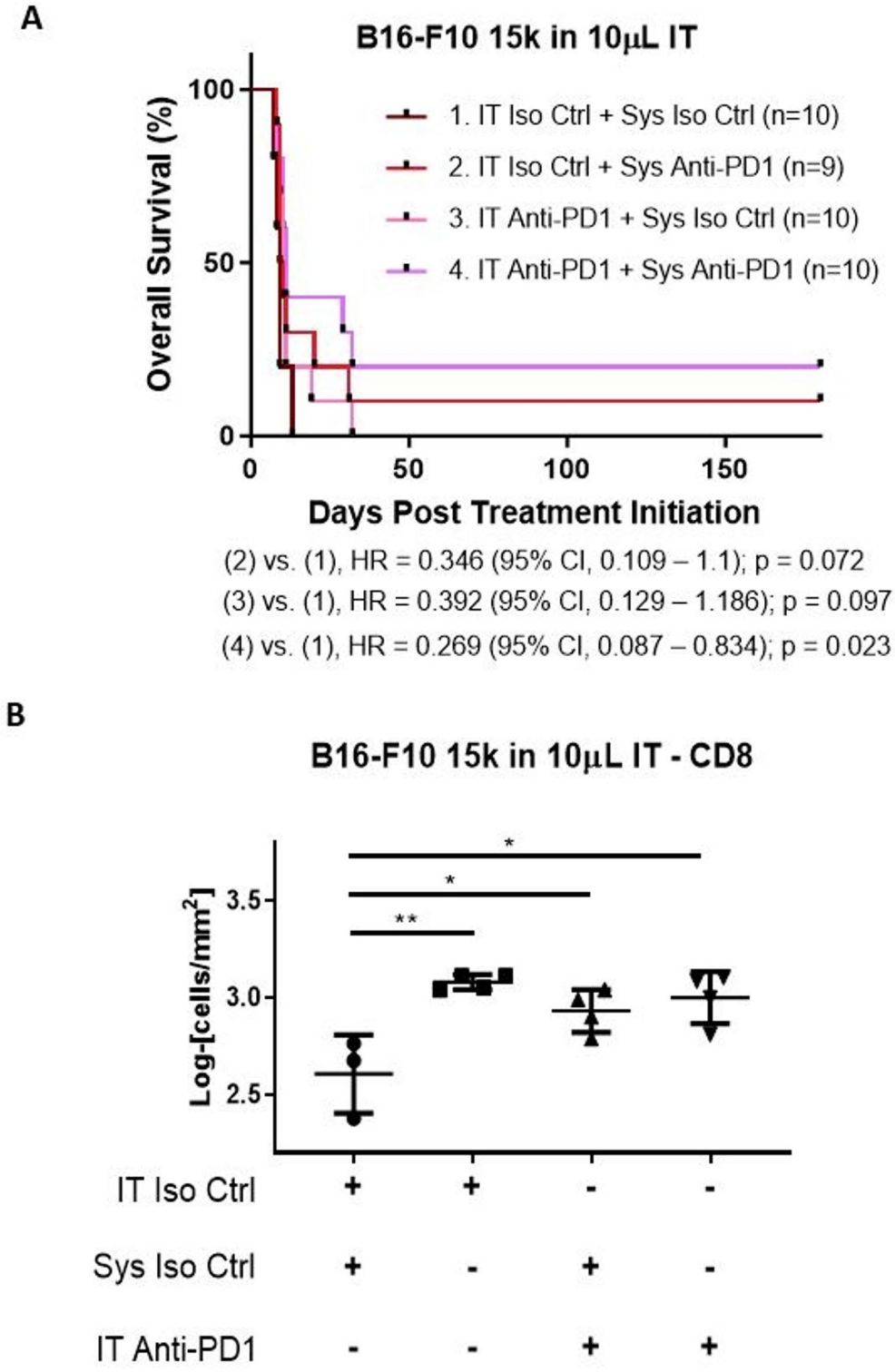

Fig. 5. Evaluation of IT anti-PD1 treatment of melanoma LMD in initial preclinical model. (**A**) Kaplan-Meier OS analysis from treatment initiation of mice that received (1) IT isotype control + systemic isotype control; (2) IT isotype control + systemic anti-PD1; (3) IT anti-PD1 + systemic isotype control; (4) IT anti-PD1 + systemic anti-PD1. Hazard ratio was determined via the Mantel-Haenszel test and significance log-rank test. (**B**) Comparison of CD8 IHC staining results between samples acquired from mice that received (1) IT isotype control l + systemic isotype control; (2) IT isotype control + systemic anti-PD1; (3) IT anti-PD1 + systemic isotype control; (4) IT anti-PD1 + systemic anti-PD1. Lines represent mean ± S.D., and each dot represents a single sample. $^{**}p < 0.01$, $^{*}p < 0.05$ by two-sided Student's *t*-test. Treatment study was performed in duplicate.

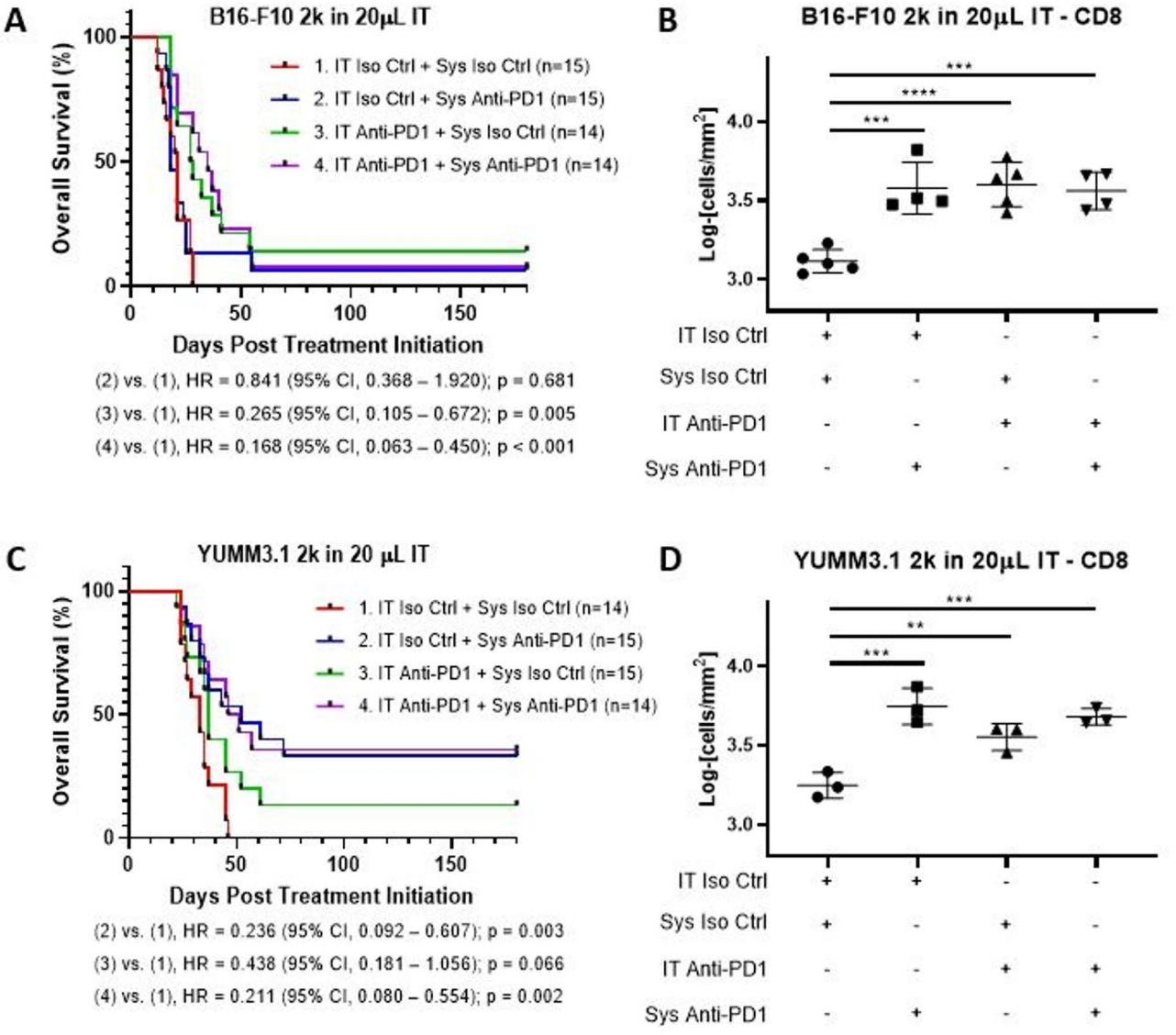

Fig. 6. Evaluation of IT anti-PD1 treatment of melanoma LMD in optimized diluted preclinical model. (**A**) B16 (2 K in 20 µL suspension condition) Kaplan-Meier analysis of (OS) from treatment initiation of mice that received: (1) IT isotype control + systemic isotype control; (2) IT isotype control + systemic anti-PD1; (3) IT anti-PD1 + systemic isotype control; (4) IT anti-PD1 + systemic anti-PD1. (**B**) Comparison of CD8 IHC staining results between samples acquired from mice that received (1) IT isotype control l + systemic isotype control; (2) IT isotype control + systemic anti-PD1; (3) IT anti-PD1 + systemic isotype control; (4) IT anti-PD1 + systemic anti-PD1. Lines represent mean ± S.D., and each dot represents a single sample. $^{**}P < 0.01$, $^{*}P < 0.05$ by two-sided Student's *t*-test. (**C**) YUM3.1 (2 K in 20ul suspension condition) Kaplan-Meier analysis from treatment initiation of mice that received treatments described in (**A**). (**D**) Comparison of CD8 IHC staining results between samples acquired from mice that received treatments described in (B). Treatment studies were performed in duplicate.

42.9% mice surviving 28 days and 14.3% surviving > 6 months. Combined treatment with IT anti-PD1 and IP anti-PD1 also improved survival versus controls (HR = 0.168, $p < 0.001$), with 57.1% mice surviving 28 days, and 7.1% mice alive > 6 months. IHC performed on brain and spinal cord tissues collected at the time mice were euthanized showed that each anti-PD1 treatment group demonstrated increased CD8 cells in the tumor deposits compared to IgG controls only (Fig. 6B**).**

We repeated this experiment using YUMM3.1 cells (Fig. 6C). Animals treated with IT and IP isotype control had a median overall survival of 33 days and all mice were euthanized by day 46. Treatment with IT anti-PD1 alone demonstrated a trend toward improved survival versus control treatment (HR = 0.438, $p = 0.066$), with 13.3% mice surviving > 6 months. IP anti-PD1 alone significantly improved survival (HR = 0.236, $p = 0.003$), with 33.3% mice surviving > 6 months. Combined treatment with IT anti-PD1 and IP anti-PD1 also improved survival compared to controls (HR = 0.211, $p = 0.002$), with 35.7% mice alive > 6 months (Fig. 6C). IHC again

demonstrated increased CD8 cells in the LMD deposits from all anti-PD1-containing treatment groups compared to the IgG control treatment (Fig. 6D).

Discussion

LMD is a severe complication of metastatic melanoma and causes significant neurological morbidity and nearly uniform mortality. Despite the significant improvements in the treatments and outcomes of metastatic melanoma patients without CNS involvement and with parenchymal brain metastases only, outcomes in melanoma patients with LMD remain extremely poor[6,19,20]. Overall, there remain very few effective treatments, or clinical trial options for patients with LMD. Progress for patients with LMD has been limited in part due to the challenges of therapeutic development for this disease entity[14,21]. The development of immunocompetent animal preclinical models is critical for the study of immune therapies for LMD.

Here, we present our experience with an orthotopic model of melanoma leptomeningeal metastasis in immunocompetent mice via cisternal injection, which can be used to investigate experimental therapeutics preclinically. Representation of clinical LMD in preclinical models is complex and requires careful consideration of multiple factors[22]. We aimed to develop LMD models that recapitulated the immune composition, genetic profile, and CSF-dissemination pattern that is observed in clinical disease. Various types of experimental mice, including immunocompetent and immunodeficient mice, have been used to model LMD from different cancer types, such as melanoma, lung, and breast cancer[13,14]. We developed LMD models in immunocompetent mice using syngeneic murine cell lines in order to evaluate immunotherapeutic treatment strategies. Specifically, we developed LMD models using cell lines with genetically relevant alterations, including oncogenic mutations in BRAF, PTEN, and/or CDKN2 as well as cell lines that underwent UV-irradiation to recapitulate mutational patterns observed in patients with melanoma[23–27].

Others have demonstrated the value of representing LMD tumor cells derived from patient CSF samples and injecting them into immunodeficient NOD scid gamma (NSG) mice[21]. This strategy for modeling LMD is compelling because it represents clonal heterogeneity existing within patient tumors and patient-derived cell lines typically have been subjected to the selective pressure of sub-culturing[28]. In addition, patient-derived circulating tumor cells from CSF samples could potentially be adapted to humanized immunocompetent mice in order to better represent the immune microenvironment[29]. While this approach has many benefits, patient-derived cells are limited due to technical challenges associated with culturing, poor growth and engraftment in vivo, potential selective pressures associated with prior exposure to therapeutics and is only feasible immunodeficient model[30]. Humanized mice models are also an option, however may be cost prohibitive in addition to facing challenges associated with tumor engraftment, and development of human immune cells[31,32]. In vivo selection of cell lines that are preferentially metastasize to the CNS, and more specifically the leptomeninges, is another avenue for LMD model development. This has been previously described for the development of brain metastasis models and now more recently for LMD[14,32]. Our approach of cisternal syngeneic cell injection in C57BL/6 mice represents another feasible framework to develop LMD models and prioritize new therapeutic approaches for patients with melanoma LMD.

For our initial LMD modeling experiments, we began with B16-F10. The aggressiveness of the B16-F10 made it a good cell line to initially identify conditions to establish gross and histological evidence of LMD. The B16-F10 LMD model offered several advantages including a high tumor take rate and reproducible survival curves. B16-F10 is pigmented so success of the model is straightforward to visualize. However, B16-F10 has some limitations. IT injection of this cell line results a short animal survival; this makes it difficult to evaluate treatment strategies as the therapeutic window is very short. B16-F10 is also poorly immunogenic, thus providing an additional challenge for assessing the benefit of IT immunotherapy[33]. Finally, B16-F10 does not carry the clinically relevant mutations and mutational diversity seen in human melanoma. To address these limitations, we evaluated multiple other syngeneic melanoma lines in an immunocompetent mouse model for their ability to grow following IT injection. We specifically evaluated both BRAF mutant and radiated lines as they have an increased mutational burden and could potentially have increased response to immunotherapy[34]. As expected, we observed cell line specific variations in survival time following IT injection. B16-F10 and RMS are known to be aggressively metastatic;[35–37] BP, D4M, and YUMM3.1 are driven by activating mutations and share BRAF activation and PTEN loss;[23–26] D4M-UV2 and MC38-gp100 may live longer due to baseline immune surveillance that results in slower disease progression[34,38]. We found the YUMMER1.7 cell line specifically to be a poor candidate as tumor take rate was very low and we observed spontaneous regression in this cell line.

We evaluated IT therapy as our experimental platform as it has a known clinical application[10–12,39]. There is a strong rationale to determine whether new immune therapies are safe and effective for patients with LMD, including with IT administration. The development and validation of preclinical models of melanoma LMD are instrumental in guiding the design of clinical trials, particularly preclinical models in immunocompetent mice. Notably, it has been postulated that immunoregulatory components of T cells may vary between the systemic and intrathecal compartments, thus supporting the need to investigate new therapies using in vivo models of LMD[40]. We observed that IT anti-PD1 treatment in mice with LMD could increase CD8 T cells in LMD deposits. Finally, we observed that combined treatment with IT and systemic anti-PD1 significantly improved survival relative to mice treated with control.

By recapitulating features of clinical LMD, these preclinical models can provide valuable insights into the efficacy and safety of novel therapeutic approaches. The translational relevance of these models lies in their ability to assess safety and potentially predict treatment responses. Insights gained from preclinical studies using these LMD models can help refine clinical trial endpoints, dosage regimens, and combination therapies, ultimately accelerating the development and translation of innovative treatments for patients with LMD.

We acknowledge that this model carries some limitations. Peri-procedural mortality presents cost-associated and logistical challenges (although we have observed reduced peri-procedural mortality with more experience

with this model). Based on our experience, the peri-procedural mortality was minimal across all cell lines but for any peri-procedural mortality that was observed, we do not believe there is an inherent increase in lethality associated with any particular melanoma cell line. Rather, the observed differences may reflect variability in experimental handling during early phases of model development. Secondly, we acknowledge that luciferase tagging may increase the immunogenicity of implanted tumor cells. However, this feature was crucial to our model design, enabling longitudinal in vivo imaging; albeit a limitation of our methodology. Lastly, while these orthotopic murine models represent a useful tool for studying LMD via tumor growth in the leptomeningeal space, as this model involves directly injecting tumor cells into the intrathecal space, this process bypasses steps in the metastatic cascade. This limits the models' ability to fully recapitulate the pathophysiology of melanoma seeding the leptomeninges. However, this model can be used as a starting point for hypothesis generation and initial safety and therapeutic evaluation, which then can be applied to other modeling systems such as in vivo selection or patient-derived models which are more expensive, complex and labor/resource intensive.

Despite these limitations, we believe that these murine melanoma LMD models provide an important resource for research and therapeutic development in this area of unmet clinical and translational need. These models are advantageous in that they are readily reproducible and emulate the dissemination pattern and progression that is observed in clinical disease. Additionally, as they are created via direct cisternal delivery of malignant cells, this model provides a "pure" LMD model not confounded by concurrent intraparenchymal or systemic disease when evaluating efficacy of treatment strategies. The intact immune system also allows for characterization of the immune microenvironment in response to the presence of leptomeningeal tumor or treatment. Overall, this model is well suited specifically for evaluation of a variety of therapeutic platforms. Future studies will evaluate other IT immune therapies to further accelerate clinical development and translation.

Conclusions

Leptomeningeal disease (LMD) is a complication of melanoma with an extremely poor prognosis and very limited treatment options. A critical limitation in the development of more effective treatments for LMD is the relative lack of preclinical models. In this study, we used orthotopic injection model system to develop several immunocompetent preclinical orthotopic models of melanoma LMD to facilitate the research and therapeutic development in this area. We also report the safety, efficacy, and immunological effects of intrathecal administration of anti-PD1 immunotherapy using this LMD model.

Data availability

All raw data will be freely available to any scientist wishing to use them for non-commercial purposes. The work described in this manuscript does not generate any new model organisms. All cell lines used for this work are murine cell lines made available by other laboratories. We are willing to share all parental and modified cell lines with any investigators that desire them. Data is provided within the manuscript or supplementary information files. Any additional data inquires can be addressed by contacting sdferguson@mdanderson.org.

Received: 22 October 2024; Accepted: 20 August 2025
Published online: 02 October 2025

References

1. Smalley, K. S. et al. Managing leptomeningeal melanoma metastases in the era of immune and targeted therapy. *Int. J. Cancer*. **139** (6), 1195–1201 (2016).
2. Cohen, J. V. et al. Melanoma central nervous system metastases: current approaches, challenges, and opportunities. *Pigment Cell. Melanoma Res.* **29** (6), 627–642 (2016).
3. Leal, T. et al. Leptomeningeal metastasis: challenges in diagnosis and treatment. *Curr. Cancer Ther. Rev.* **7** (4), 319–327 (2011).
4. Le Rhun, E., Taillibert, S. & Chamberlain, M. C. Carcinomatous meningitis: leptomeningeal metastases in solid tumors. *Surg. Neurol. Int.* **4** (Suppl 4), S265–S288 (2013).
5. Garcia Molina, E. & Penas-Prado, M. Neoplastic meningitis in solid tumours: updated review of diagnosis, prognosis, therapeutic management, and future directions. *Neurologia (Engl Ed)*. **37** (9), 794–805 (2022).
6. Ferguson, S. D. et al. Predictors of survival in metastatic melanoma patients with leptomeningeal disease (LMD). *J. Neurooncol.* **142** (3), 499–509 (2019).
7. Goldberg, S. B. et al. Pembrolizumab for management of patients with NSCLC and brain metastases: long-term results and biomarker analysis from a non-randomised, open-label, phase 2 trial. *Lancet Oncol.* **21** (5), 655–663 (2020).
8. Long, G. V. et al. Combination nivolumab and ipilimumab or nivolumab alone in melanoma brain metastases: a multicentre randomised phase 2 study. *Lancet Oncol.* **19** (5), 672–681 (2018).
9. Tawbi, H. A. et al. Safety and efficacy of the combination of nivolumab plus ipilimumab in patients with melanoma and asymptomatic or symptomatic brain metastases (CheckMate 204). *Neuro Oncol.* **23** (11), 1961–1973 (2021).
10. Glitza, I. C. et al. Retrospective review of metastatic melanoma patients with leptomeningeal disease treated with intrathecal interleukin-2. *ESMO Open.* **3** (1), e000283 (2018).
11. Glitza Oliva, I. C. et al. Concurrent intrathecal and intravenous nivolumab in leptomeningeal disease: phase 1 trial interim results. *Nat. Med.*, (2023).
12. Glitza, I. C. et al. M. Concurrent intrathecal (IT) and intravenous (IV) nivolumab (N) for melanoma (MM) patients (pts) with leptomeningeal disease (LMD). in ESMO Congress 2023. Madrid, Spain: Annals of Oncology. (2023).
13. Reijneveld, J. C., Taphoorn, M. J. & Voest, E. E. A simple mouse model for leptomeningeal metastases and repeated intrathecal therapy. *J. Neurooncol.* **42** (2), 137–142 (1999).
14. Boire, A. et al. Complement component 3 adapts the cerebrospinal fluid for leptomeningeal metastasis. *Cell* **168** (6), 1101–1113e13 (2017).
15. Remsik, J. et al. Characterization, isolation, and in vitro culture of leptomeningeal fibroblasts. *J. Neuroimmunol.* **361**, 577727 (2021).
16. Remsik, J. et al. Leptomeningeal anti-tumor immunity follows unique signaling principles. *BioRxiv*, (2023).
17. Feoktistova, M. et al. Crystal Violet assay for determining viability of cultured cells. *Cold Spring Harb Protoc.*, (4): (2016). pdb.prot087379

18. Peng, W. et al. Transduction of tumor-specific T cells with CXCR2 chemokine receptor improves migration to tumor and antitumor immune responses. *Clin. Cancer Res.* **16** (22), 5458–5468 (2010).
19. Chorti, E. et al. Leptomeningeal disease from melanoma-Poor prognosis despite new therapeutic modalities. *Eur. J. Cancer*. **148**, 395–404 (2021).
20. Nguyen, A. et al. Leptomeningeal metastasis: A review of the pathophysiology, diagnostic methodology, and therapeutic landscape. *Curr. Oncol.* **30** (6), 5906–5931 (2023).
21. Law, V. et al. A preclinical model of patient-derived cerebrospinal fluid Circulating tumor cells for experimental therapeutics in leptomeningeal disease from melanoma. *Neuro Oncol.* **24** (10), 1673–1686 (2022).
22. Huszthy, P. C. et al. Vivo models of primary brain tumors: pitfalls and perspectives. *Neuro Oncol.* **14** (8), 979–993 (2012).
23. Peng, W. et al. Loss of PTEN promotes resistance to T Cell-Mediated immunotherapy. *Cancer Discov.* **6** (2), 202–216 (2016).
24. Cooper, Z. A. et al. Response to BRAF Inhibition in melanoma is enhanced when combined with immune checkpoint Blockade. *Cancer Immunol. Res.* **2** (7), 643–654 (2014).
25. Meeth, K. et al. The YUMM lines: a series of congenic mouse melanoma cell lines with defined genetic alterations. *Pigment Cell. Melanoma Res.* **29** (5), 590–597 (2016).
26. Jenkins, M. H. et al. Multiple murine BRaf(V600E) melanoma cell lines with sensitivity to PLX4032. *Pigment Cell. Melanoma Res.* **27** (3), 495–501 (2014).
27. Cancer Genome Atlas, N. Genomic classification of cutaneous melanoma. *Cell* **161** (7), 1681–1696 (2015).
28. Hughes, P. et al. The costs of using unauthenticated, over-passaged cell lines: how much more data do we need? *Biotechniques* **43** (5), 575–577 (2007).
29. Allen, T. M. et al. Humanized immune system mouse models: progress, challenges and opportunities. *Nat. Immunol.* **20** (7), 770–774 (2019).
30. Francia, G. et al. Mouse models of advanced spontaneous metastasis for experimental therapeutics. *Nat. Rev. Cancer*. **11** (2), 135–141 (2011).
31. Walsh, N. C. et al. Humanized mouse models of clinical disease. *Annu. Rev. Pathol.* **12**, p187–215 (2017).
32. Valiente, M. et al. Brain metastasis cell lines panel: A public resource of organotropic cell lines. *Cancer Res.* **80** (20), 4314–4323 (2020).
33. Becker, J. C. et al. Mouse models for melanoma: a personal perspective. *Exp. Dermatol.* **19** (2), 157–164 (2010).
34. Lo, J. A. et al. Epitope spreading toward wild-type melanocyte-lineage antigens rescues suboptimal immune checkpoint blockade responses. Sci Transl Med, 13(581). (2021).
35. Fidler, I. J. & Nicolson, G. L. Organ selectivity for implantation survival and growth of B16 melanoma variant tumor lines. *J. Natl. Cancer Inst.* **57** (5), 1199–1202 (1976).
36. Overwijk, W. W. & Restifo, N. P. B16 as a mouse model for human melanoma. Curr Protoc Immunol, 2001. Chapter 20: p. Unit 20 1.
37. Ben Baruch, B. et al. Stromal CD38 regulates outgrowth of primary melanoma and generation of spontaneous metastasis. *Oncotarget* **9** (61), 31797–31811 (2018).
38. Peng, W. et al. PD-1 Blockade enhances T-cell migration to tumors by elevating IFN-gamma inducible chemokines. *Cancer Res.* **72** (20), 5209–5218 (2012).
39. Palmisciano, P. et al. Intrathecal therapy for the management of leptomeningeal metastatic disease: a scoping review of the current literature and ongoing clinical trials. *J. Neurooncol.* **160** (1), 79–100 (2022).
40. Freedman, M. S. et al. Immunoregulatory properties of T-cell lines derived from the systemic and intrathecal compartments: a phenotypic and functional study. *Ann. Neurol.* **27** (3), 258–265 (1990).

Author contributions

Conception and design: RAG, GMF, MAD, SDF; Acquisition of data: RAG, GMF, JRC, BGK, CWH, YFD, QH CYBO, FCLC, MTT, JTH, SDF; Analysis and interpretation of data: RAG, GMF, DAL, FCLC, MTT, JTH, ICG, MAD, SDF; Writing, review, and/or revision of the manuscript: All authors; Study supervision: RAG, GMF, MAD, SDF.

Funding

RAG and GMF received research funding from the NIH National Center for Advancing Translational Sciences (TL1TR0003169 and UL1TR003167). GMF received additional support from The University of Texas MD Anderson Cancer Center (MD Anderson)/UTHealth Graduate School of Biomedical Sciences' Caroline Ross Fellowship, Schissler Foundation Fellowship, and Presidents' Research Scholarship. JTH is supported by the American Cancer Society (RSG-16-179-01-DMC) and NCI (R01 CA240338, R01 CA232754). MAD is supported by the Dr. Miriam and Sheldon G. Adelson Medical Research Foundation, the AIM at Melanoma Foundation, the NIH/NCI P50CA221703, the American Cancer Society and the Melanoma Research Alliance, Cancer Fighters of Houston, the Anne and John Mendelsohn Chair for Cancer Research, and philanthropic contributions to the Melanoma Moon Shots Program of MD Anderson. SDF is supported by the MD Anderson Melanoma Moon Shots Program and Melanoma Research Alliance and a Career Enhancement Program award from the MD Anderson SPORE in Melanoma (NIH/NCI P50CA221703).

Declarations

Competing interests

The authors declare no competing interests.

Consent for publication

All authors agree with publication.

Ethics approval

The Institutional Animal Care and Use Committee at MD Anderson Cancer Center approved all procedures involving mice in this study (Davies Protocol 00000743-RN02).

Additional information

Supplementary Information The online version contains supplementary material available at https://doi.org/10.1038/s41598-025-16889-3.

Correspondence and requests for materials should be addressed to S.D.F.

Reprints and permissions information is available at www.nature.com/reprints.

Publisher's note Springer Nature remains neutral with regard to jurisdictional claims in published maps and institutional affiliations.